Dynamic transport and reaction behaviour of high-pressure gases in high-rank coal

Renato Zagorščak[a]* and Hywel Rhys Thomas[a]

[a] Geoenvironmental Research Centre (GRC), School of Engineering, Cardiff University, The Queen's Buildings, The Parade, Cardiff, CF24 3AA

*corresponding author (ZagorscakR@cardiff.ac.uk)

Abstract:

This paper presents the results obtained through continuous and simultaneous measurements of gas flow, temperature and coal deformation during high-pressure gas injection in high-rank coal samples, obtained from the South Wales coalfield (UK). The results demonstrate that CO_2 flow rates experience an initial decline due to internal coal swelling, followed by the flow rate recovery and global coal swelling. As the flow of high-pressure CO_2 induces measurable temperature drop within the sample related to the Joule-Thomson cooling, the changes induced by the variations in thermal state of the system are associated with abrupt shift in coal response to reactive gas flow. However, subsequent injections of He and N_2 show that the changes induced by CO_2 sorption on coal permeability to gases are irreversible. This work demonstrates the importance of considering the coupled reactive gas and heat transport, and consequent coal deformation mechanisms while assessing the storage potential of coal seams.

Keywords: Coal; Carbon sequestration; Permeability; CO_2 sorption; Swelling; Joule-Thomson effect.

1. Introduction

From the beginning of the 1st industrial revolution until today, around 2040±310 Gt of anthropogenic CO_2 has been emitted to the atmosphere, whereas about half of it being released in the last 40 years (IPCC, 2014). Based on the recent report by the IPCC (2018) and The Royal Academy and Royal Academy of Engineering (2018), storing of around 810 Gt of CO_2 until 2100 will be required to limit the rise in temperature to 1.5°C compared to pre-industrial times.

Carbon Capture and Storage (CCS) is a technology that can deliver significant emissions reductions from the fossil fuels use (IEA, 2016). Sequestering the CO_2 in the coal beds that cannot be mined is an attractive option as it allows the production of methane, a value-added product, which has been confirmed in several international pilot projects and experimental investigations (White et al., 2005; Wang et al., 2015). However, as the coal is known to swell upon CO_2 adsorption, the swelling associated loss in permeability is the main technical challenge that needs to be overcome to perform a successful large-scale CO_2 enhanced coal bed methane (CO_2-ECBM) project (Wong et al., 2007; van Bergen et al., 2009; Fujioka et al., 2010).

Laboratory investigations have demonstrated that in general, the permeability of coal to gases decreases with an increase in effective stress (Durucan and Edwards, 1986; Pan et al., 2010; Chen et al., 2011; Li et al., 2013; Alexis et al., 2015; Meng et al., 2015; Vishal, 2017). In the case of CO_2 injection, Pan et al. (2010) and Jasinge et al. (2011) have shown that coal permeability to CO_2 decreases with an increase in confining pressure and pore pressure, the latter being associated directly with adsorption-induced coal swelling. Similarly, Perera et al. (2011) and Ranathunga et al. (2017) have demonstrated on low rank coals that there is a higher decline in permeability with increasing injection pressure when CO_2 is in its supercritical state ($scCO_2$). However, it was noted that injecting N_2 could reverse some of the swelling effects caused by the $scCO_2$ adsorption (Perera et al., 2011; Ranathunga et al., 2017). Such experimental results have given detailed insights on the permeability evolution with respect to the stress state of coal or gas pressure, however the time-dependent flow and deformation experimental data that could provide further insights into the coupled thermal-gas-mechanical processes were commonly omitted. As suggested by Liu et al. (2011) and Qu et al. (2012; 2014), permeability varies considerably during the adsorption process and the current measurements and results do not involve dynamic processes, hence, not reflecting the real permeability evolution, i.e. dynamic flow of gas under the effects of CO_2 induced matrix swelling induced by pressure and temperature changes. Several studies have presented the time-dependent data, however, predominantly on understanding the gas pressures and concentrations in the context of ECBM (e.g. Zhou et al., 2013; Wang et al., 2015), or dealing with correlations between the coal swelling and permeability during isothermal gas injection (e.g. Mazumder and Wolf; 2008; Wang et al., 2010; Liu et al., 2016).

Gas flow measurements are frequently conducted under the assumption of isothermal conditions without measuring the temperature directly on the samples, despite the fact that some gases can experience cooling or heating effects during expansion under the pressure gradient or generate heat as a result of the adsorption process which is known to be an exothermic reaction (Ozdemir et al., 2004; Oldenburg, 2007, Yue et al., 2015). In particular, for conditions relevant to carbon capture and sequestration, Kazemifar and Kyritsis (2014) have experimentally demonstrated that CO_2 experienced the Joule-Thomson cooling of approximately 0.5 °C/bar. Furthermore, it is well-known that CO_2 sorption and swelling are temperature dependent, i.e. increase with a decrease in temperature (Krooss et al., 2002; Li et al., 2010, Baran et al., 2015). In particular, the observable CO_2 induced volumetric strain has doubled for a temperature drop of 25°C, as shown by Baran et al. (2015). Hence, the effect of Joule-Thomson cooling could affect the injectivity in CCS projects by disturbing the equilibrium of the coal-gas system (Oldenburg, 2007). According to the author's knowledge there has been no attempt so far to measure dynamic temperature changes across the coal sample and assess the effect of CO_2 cooling during continuous high-pressure CO_2 injection on coal behaviour.

In regards to the CO_2 sorption associated swelling where a large portion of researchers has dealt with coal swelling measurements on unconfined coal samples, Levine (1996), Day et al. (2008), Battistutta et al. (2010) have shown that coal samples exposed to CO_2 did not show any irreversible effects. On the contrary, Majewska et al. (2009) and He et al. (2010) have shown that CO_2 induced swelling was not fully reversible leaving the coal samples with higher volumes compared to the original values. Gathitu et al. (2009), Hol et al., (2012a;2014) and Vishal et al. (2015) have reported that CO_2 induced swelling causes crack initiation and creation of micro-fractures. Such phenomenon was considered to be irreversible by Liu et al. (2015). Hence, the reversibility of CO_2 sorption induced effects and their impact on coal transport properties are still open to discussion.

This paper therefore investigates the reactive gas transport in two high rank intact coal samples, obtained from the South Wales Coalfield, UK under constant stress conditions (10.0 MPa confining pressure) and high-pressure gas injections (7.0-8.0 MPa injection pressures). Sample A contains multiple embedded fractures while sample B exhibits poor fracture network. Two multi-day investigations involve the injection of He, CO_2 and N_2 under different experimental conditions where confining and gas pressures, gas flow rates, displacements in radial and axial directions as well as the sample temperatures are recorded continuously. First, a sequential injection of He, CO_2 and again, He is conducted on both samples. Additionally, sample B is then further treated with N_2 and He. The results obtained during the initial injection of He represent the baseline information on gas flow and coal deformation. The primary objective of injecting CO_2 and N_2 is twofold. Firstly, to investigate the effect of CO_2 injection and the associated effects on the coal behaviour and secondly, to assess the effect of N_2 sorption on the reversal of changes induced by CO_2. Such impacts are assessed using the second and third He injections, respectively.

2. Methodology

2.1. Samples

Coal samples were collected from the 9ft coal seam in South Wales coalfield, UK from depth of 150 m (Zagorščak, 2017; Zagorščak and Thomas, 2018; 2019). The blocks of coal, locally known under the name of Black Diamond (BD), have been extracted from the East Pit East opencast coal mine and used to extract coal cores, 70 mm in diameter (Fig. 1). Coal samples were air-dried prior to the experiments and characterisation tests (ASTM D3302/D3302M, 2015).

Fig. 1. Coal lump obtained to extract the coal samples by core drilling.

Based on a visual inspection of the samples extracted, one sample with well-developed fracture network (sample A) and one with poor cleat system (sample B) were chosen (Fig. 2). Table 1 presents the dimensions and physical properties of the samples, while Table 2 shows the coal characteristics based on the results of Proximate and Ultimate analyses (Zagorščak, 2017). By comparing the results obtained with the ASTM D388 (2015) classification of coal rank, BD coal can be classified as a high rank anthracitic coal.

Table 1
Sample information of the coal used in the study.

Sample ID	Mass (g)	Diameter (cm)	Height (cm)	Density (g/cm^3)
Sample A	578.8	6.96	11.07	1.373
Sample B	484.2	6.95	9.24	1.382

Table 2
Results of the Proximate and Ultimate analyses.

Moisture content (%)	Ash Content (%)	Volatile matter (%)	Total carbon content (%)	Total sulphur content (%)
1.65 ± 0.12	1.65 ± 0.38	5.82 ± 0.21	90.12 ± 0.11	0.95 ± 0.02

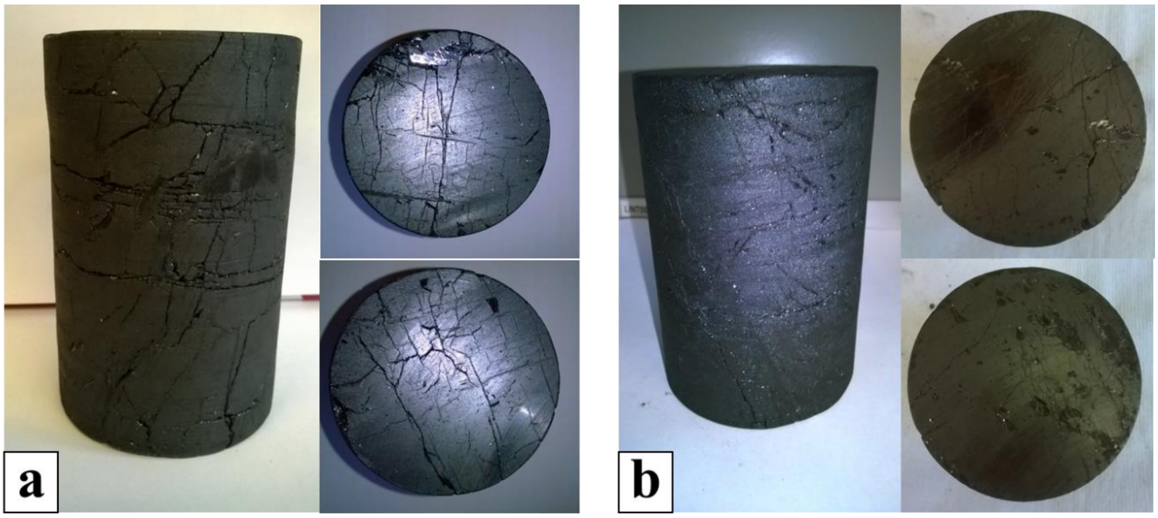

Fig. 2. Coal cores used in the study; a) sample A, b) sample B.

2.2. Experimental setup and measurements methods

2.2.1. Experimental apparatus

The experimental apparatus used in this work can be applied to conduct measurements of rock deformation and gas flow, by applying pressures up to 20 MPa and temperatures up to 338K. The confining stresses, injection pressures and backpressures, radial and axial displacements of the sample as well as the temperature at multiple locations across the samples can be continuously recorded using the setup. The setup consists of: i) the triaxial cell, ii) pressure and temperature control units, iii) flow, pressure, displacement and temperature measurement units and iv) the gas supply system (Fig. 3).

In the triaxial cell manufactured by GDS Instruments, which can accommodate samples up to 0.07 m in diameter and 0.2 m in length, each core sample was first wrapped in a PTFE tape and then placed between triaxial base and top cap. Porous disks, 0.6 mm in thickness, were inserted between the sample and the end plates. A silicone rubber sleeve with a thickness of 1.5 mm was placed around the samples and porous discs, and then secured to the cell base and top cap using “O” rings and stainless-steel hose clips.

A top cover of the triaxial cell was then placed on the base of the cell and filled with silicone hydraulic oil 350 Polydimethylsiloxane. Using the GDS Instruments pressure/volume controller, confining pressure of 3.0 MPa was applied. Vacuuming of each sample, using a Buchi vacuum pump, was conducted for 24 hours before each experiment.

Pressurisation of CO_2 to the required experimental pressures and injection in the triaxial cell was achieved using a dual syringe Teledyne Isco 500D pump system, connected to a liquid withdrawal CO_2 cylinder. Temperature of the pumps was controlled by circulating the deionised water through heating jackets via the Huber Pilot One Ministat 125 temperature controller. He and N_2 experiments were conducted using a highly pressurised gas directly from the respective cylinders. The backpressure in the system was controlled using a Swagelok backpressure regulator.

Two digital Bronkhorst mass flow meters and two in-line GDS Instruments pore pressure transducers measured the upstream and downstream flow rates and gas pressures, respectively. Four heating elements, controlled by the GDS temperature controller, were wrapped around the top cover of the triaxial cell aiming to ensure constant temperature conditions inside the cell during each experiment. For the same purpose, glass-fibre heater tapes, controlled by a digital three-zone temperature controller, were placed around the pipeline. GDSLab software was used to continuously monitor pressures, temperatures and flow rates by recording high-resolution data every ten seconds.

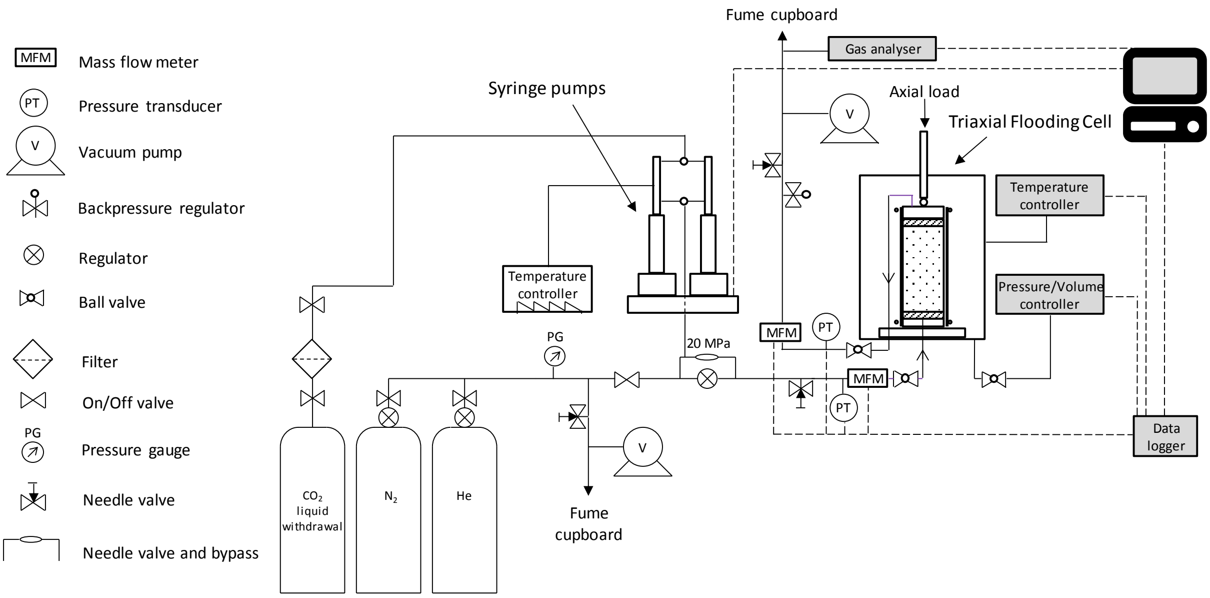

Fig. 3. A schematic diagram of the experimental setup.

2.2.2. Gas flow and permeability measurements

The injection sequences used to subject the coal samples to different gases are shown in Table 3. First, He was injected in both samples to assess the coal's response to inert, non-sorbing gas and to use the results as a baseline for subsequent gas injections. CO_2 was injected then, followed by re-injection of He to investigate the influence of CO_2 sorption related effects on coal behaviour. N_2 and He were additionally injected in sample B to analyse the impact of N_2 sorption on the reversal of changes induced by CO_2. During the first four hours of each He and CO_2 sequence, confining and gas pressures were gradually building up from the initial state, i.e. 3.0 MPa and atmospheric pressure to the designed values shown in Table 4, respectively. After that, only the upstream gas pressures were further increased while keeping the confining pressures and the downstream gas pressures constant. N_2 was injected in the sample under the conditions specified in Table 4 and kept in the sample for 48 hours. After each injection sequence, all pressure values were restored to the initial state after which the system has been degassed for 48 hours.

As shown in Table 4, minimum average gas pressures used within samples A and B are 4.75 MPa and 3.75 MPa, respectively. The Klinkenberg (slip flow) effect in high rank coal becomes negligible for average gas pressures above 2 MPa (e.g. Chen et al., 2011; Zagorščak and Thomas, 2016), hence it is not considered in this study.

Table 3

Gas injection sequences performed in the study.

Sample ID	Injection sequences				
Sample A	1st Helium injection	Carbon dioxide injection	2nd Helium injection	-	-
Sample B	1st Helium injection	Carbon dioxide injection	2nd Helium injection	Nitrogen	3rd Helium injection

Table 4

Pressure conditions during the gas flow measurement tests.

Sample ID	**Helium and Carbon dioxide injections**					**Nitrogen injection**		
	Confining pressure (MPa)	**Injection Pressure (MPa)**			**Backpressure (MPa)**	**Confining pressure (MPa)**	**Injection pressure (MPa)**	**Backpressure (MPa)**
		1st step	**2nd step**	**3rd step**				
Sample A	10.0	7.0	7.5	8.0	2.5	-	-	-
Sample B	10.0	7.0	7.5	8.0	0.5	10.0	5.4	4.0

Coal permeability to gases was determined using a steady-state flow method and applying the Darcy's equation for compressible gases to calculate the permeability values (Durucan and Edwards, 1986):

$$K_g = \frac{2P_0Q_gL\mu_g}{A(P_1^2 - P_2^2)} \tag{1}$$

where K_g is the measured permeability to gas (m^2), Q_g is the volumetric flow rate (m^3/s), P_0 is the gas pressure at which Q_g is measured (Pa), L is the sample length (m), μ_g is the gas viscosity (Pa.s), A is the cross-sectional area (m^2), P_1 and P_2 are the upstream and downstream gas pressures (Pa), respectively. The mass flow rates measured using the Bronkhorst mass flow meters have been converted into the volumetric flow rates taking into account density of the gas corresponding to the pressure and temperature determined at the downstream of the sample.

The temperature of the experimental system was set at 310±1K (37±1°C) representing in-situ conditions up to 800 m of depth, where CO_2 exists in supercritical form, under the assumption of an average hydrostatic gradient of 0.01 MPa/m and an average thermal gradient of 0.03 K/m (°C/m) with an average surface temperature of 285K (12°C).

2.2.3. Deformation and temperature measurements

Coal deformation was measured through two axial and one radial strain transducers, provided by GDS Instruments, capable of measuring deformation up to 0.0001 mm (Fig. 4). Based on the results obtained, the volumetric strain is approximately determined by adding two radial strains to the axial strain (Pan et al., 2010). Temperature values close to the upstream and downstream of the samples were measured by fixing the thermocouples directly on the silicone sleeve at the opposite sides of each sample, 2 cm from the sample ends.

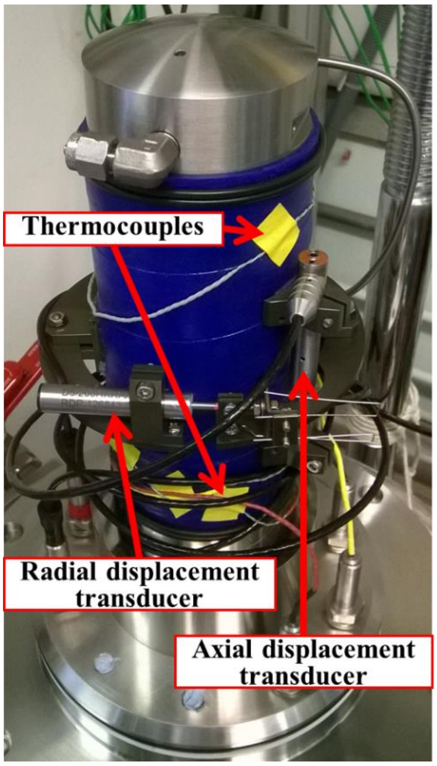

Fig. 4. Location of the thermocouples and displacement transducers.

3. Experimental results and discussion

3.1. Flow and deformation behaviour

3.1.1. Injection of Helium

Analysing the results obtained during the 1st He injection presented in Fig. 5, one can observe that during the first four hours of each experiment, flow rates were continuously increasing, despite the fact that the confining pressures were increased by 7.0 MPa (from 3.0 MPa to 10.0 MPa) in both samples compared to the mean gas pressures which were increased by 4.75 MPa in sample A and by 3.75 MPa in sample B. This confirms that the same amount of change of either pore gas pressure or confining stress does not have the same impact on flow behaviour, as suggested previously by Chen et al. (2011).

After the injection pressures were increased to the designed values, a constant flow rate condition was achieved within half an hour. As He is a non-sorbing gas, which is assumed to assess the same pore volume as CO_2 (e.g. Mohammad et al., 2009; Zagorščak and Thomas, 2019), it can easily penetrate the fractures and microporous coal matrix, allowing the steady-state condition to be achieved relatively fast. In particular, steady-state flow rates of 24 g/h and 3 g/h were measured in samples A and B at the end of the first injection step (7.0 MPa), respectively. Upon increasing the injection pressures to 7.5 MPa and 8.0 MPa, flow rates also increased to 32 g/h and 43 g/h for sample A and to 4 g/h and 6 g/h for sample B, respectively. Those results demonstrate that sample A is up to 8 times more permeable than sample B.

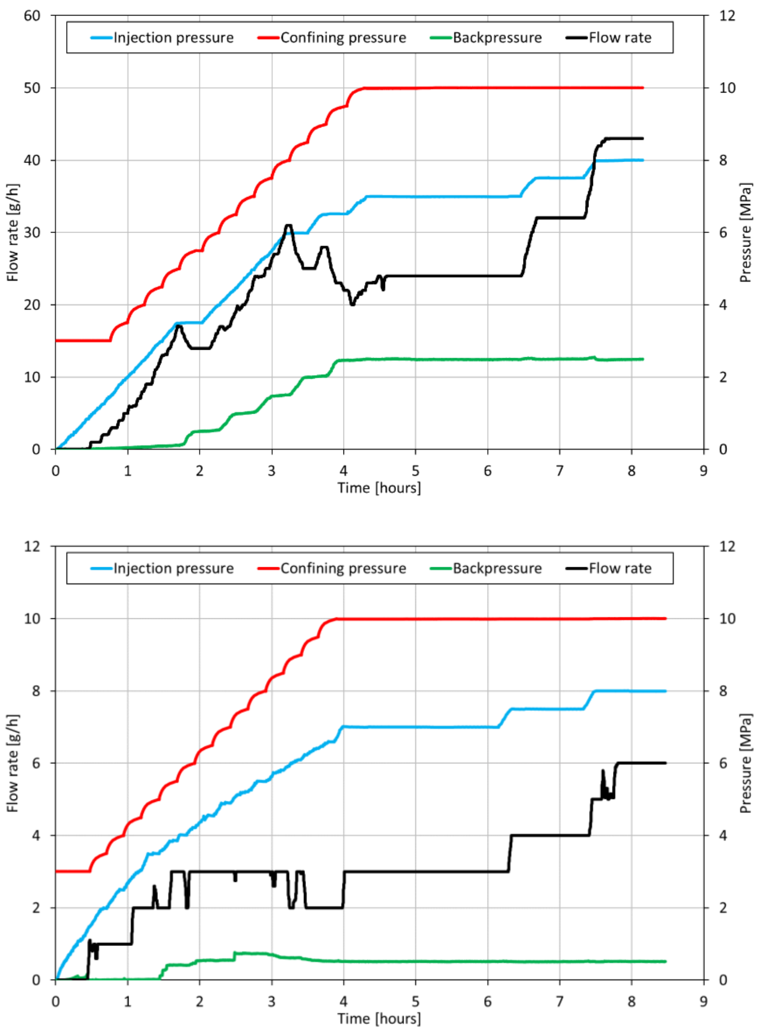

a)

b)

Fig. 5. Gas and confining pressures, and flow rates measured during the 1st helium injection; a) sample A, b) sample B.

To predict the behaviour of a coal reservoir during gas injection, the mechanisms controlling the transport of gases in the pore system of coals need to be understood. It is generally accepted that mechanisms in coal operate at two different pore scales (Prinz and Littke, 2005; Hol et al., 2011; Cai et al., 2013). In the cleat system, gas exists as a free fluid where it fills and pressurises the system having a mechanical effect which is commonly described by poroelastic theory where the volume changes occur due to changes in fluid pressure (Biot, 1941; Hol et al., 2011). Under such conditions, molecular interactions between the coal and gas are neglected and a Darcy-type flow is expected to occur through the cleats (Hol et al., 2011). In the coal matrix consisting of small pores and nanoscale voids, gas is driven by intermolecular forces which influence diffusion and adsorption (Hol et al., 2011). In the case of He injection, sorption is assumed to be negligible as it is measured in units of $\mu mol\ g^{-1}$ compared to $mmol\ g^{-1}$ for CO_2 which is known to be strongly associated with adsorption in the coal's microporous matrix where molecular interactions associated with adsorption induce coal swelling changing the stress state and permeability of the confined coal reservoir (Day et al., 2008; Sakurovs et al., 2009; Hol et al., 2011; Wang et al., 2015).

Hence, grain compressibility and the consequent increase in fracture aperture are the main mechanisms for an observed increase in flow rates with an increase in He injection pressure. As He is a non-sorbing gas, the changes in cleat aperture associated with matrix swelling can be considered negligible. Furthermore, although coal is a weak rock, coal grain compressibility is larger than expected, particularly at high pore pressures (Chen et al., 2011). Therefore, by keeping the confining and downstream pressures constant, an increase in injection pressures resulted in decreasing the effective stress, compression of coal grains and widening the flow pathways by increasing the flow rates in turn.

The differences in the results between the samples are primarily related to the coal structure and the mean gas pressures applied in each sample. Contrary to sample B, sample A exhibits a well-developed fracture network that allows easy access to the gas molecules, as shown in Fig. 2. Furthermore, applying a higher backpressure in sample A (2.5 MPa) compared to sample B (0.5 MPa) resulted in a higher mean gas pressure, i.e. lower effective stress within sample A.

Fig. 6 shows the radial and axial strains measured on both samples. During the first hour of each experiment, the radial expansion is negligible while each sample expands in the axial direction. Such expansion was caused by higher increase in injection pressures compared to an increase in confining stresses within the same period, allowing sample expansion as a result of increasing the fracture pore space. After that and by the end of the fourth hour of each experiment, until the pressures were raised to the designed values, both samples experienced continuous axial and radial compressions. Hence, within that period, an increase in confining stress had more impact on sample deformation than an increase in mean gas pressure. However, as the loss in flow rates (Fig. 5) is not as pronounced as the sample compression (Fig. 6) during the first four hours of each experiment, this implies that closure of both isolated, dead-end fractures as well as the ones available for flow is responsible for sample volume reduction.

Taking axial strains measured during the initial increase in confining stress from 3.0 MPa to the predetermined value of 10.0 MPa as a reference point, i.e. -0.023% for sample A and -0.015% for sample B, samples A and B expanded in axial direction by 0.005% and 0.019% for 1 MPa of gas pressure increase, respectively. Apart from the radial compression of -0.081% for sample A and -0.062% for sample B during the first four hours of the experiments when the pressures were raised to the designed values, samples experienced negligible radial deformation as a result of further injection pressure increase. The difference in radial and axial strains is related to the fact that coals show anisotropic deformation influenced by the anisotropy of the mechanical properties and structure of coals and cleating (Pan and Connell, 2011; Anggara et al., 2016), where expansion perpendicular to the bedding is higher than the expansion measured in direction parallel the bedding plane (Day et al., 2010; Hol and Spiers, 2012). The anisotropy also depends on confining pressure applied, where increasing the confining pressure can minimise the anisotropy (Wang et al., 2013).

Although sample A is more permeable than sample B, the latter one experienced up to four times higher axial strain than the former one for the same change in injection pressure. This was also reflected in the flow behaviour where flow rates in sample B increased by 100% when the injection pressure increased by 1 MPa, compared to an increase by 80% in sample A. Such results show that the role of He injection pressure on flow and deformation behaviour was higher in sample B compared to sample A.

In general, the volumetric behaviour is related to the poroelastic response of the coal structure when there is no interaction between the solid coal material and pore fluid phase (Hol et al., 2012b). More specifically, changes in axial and radial strains are proportional to the amount of fluid injected in the sample (Biot, 1941; Hol et al., 2011). In other words, as an increase in the amount of gas flowing through the sample pressurises the fracture system and no sorption occurs in the case of He injection, a consequent increase in volumetric expansion of the sample is primarily correlated to the increase in the fracture volume occupied by the gas.

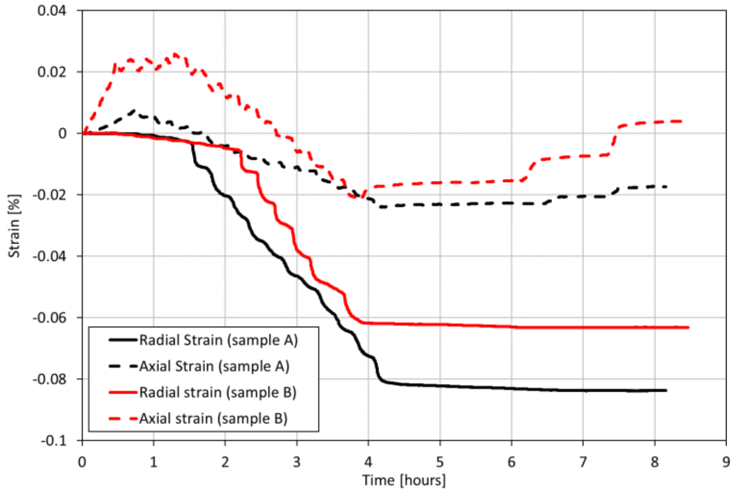

Fig. 6. Axial and radial strains determined during the 1st helium injection on both samples.

3.1.2. Injection of carbon dioxide

The steady-state condition of CO_2 flow rates and displacements in both samples was achieved within a minimum period of five hours during each injection step, with the exception of the third injection step in Sample A (Fig. 7 and Fig. 8). The reason is related to the fact that the CO_2 injection had to be stopped after 35 hours as the maximum displacement capacity of the oil pressure controller had been reached while trying to accommodate the expansion of sample A.

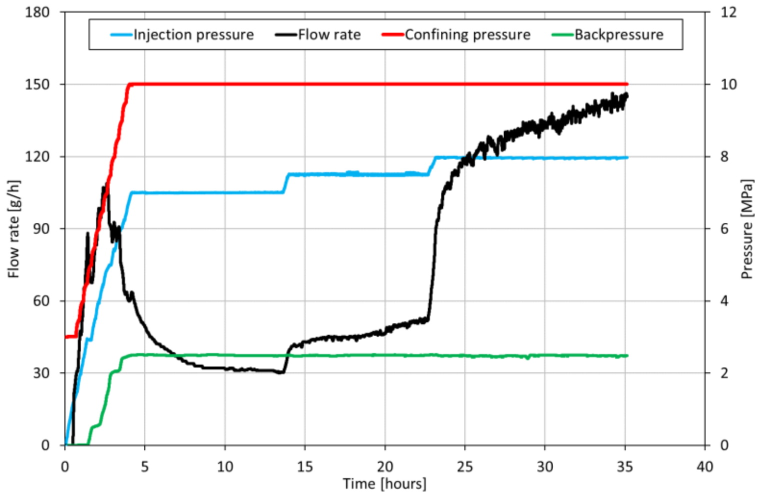

a)

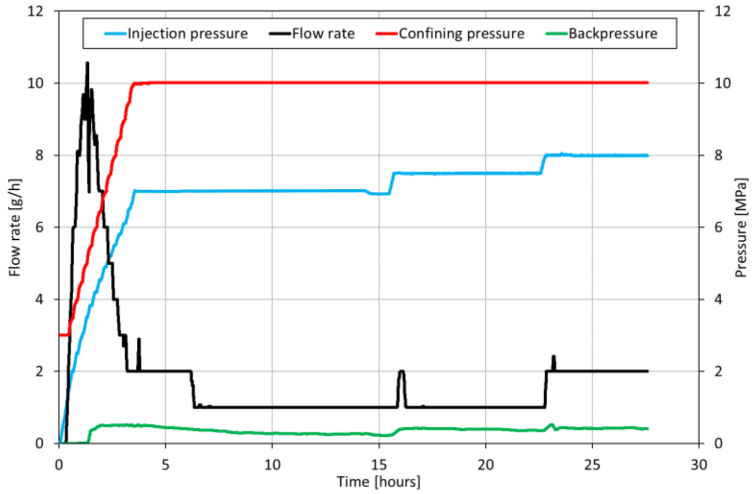

b)

Fig. 7. Gas and confining pressures, and flow rates measured during carbon dioxide injection; a) sample A, b) sample B.

The results reveal that in the period when the upstream, downstream and confining pressures were being increased to the designed values, flow rates increased to a maximum of 110 g/h for sample A and 11g/h for sample B during the first 2 hours and then experienced a reduction reaching a minimum of 31 g/h for sample A and 1 g/h for sample B at the end of the first injection step (7.0 MPa). Increasing the injection pressure to 7.5 MPa partially recovered the flow rate in sample A only, reaching a value of 52 g/h. Increasing the injection pressure to 8.0 MPa initiated the flow rate recovery in both samples, resulting in maximum flow rates of 142 g/h in sample A and 2 g/h in sample B. Hence, it can be inferred that sample A conducted up to 70 times more gas than sample B, which is nine times higher than what has been observed in the case of He injection.

As a result of CO_2 sorption induced coal swelling, radial strains of 0.18%, 0.30% and 0.78% were measured on sample A and 0.42%, 0.60% and 0.85% on sample B at the end of the first, second and third injection steps, respectively (Fig. 8). During the same steps, axial strains of 0.04%, 0.13% and 0.17% were determined on sample B, respectively. However, sample A expanded axially only in the last injection step by 0.19%. Therefore, one can infer that applying a constant confining stress of 10 MPa offered only a partial constraint to the coal, i.e. the swelling pressure exceeded the value of the confining pressure allowing the coal to swell freely.

The volumetric response of coal as well as the flow behaviour observed here are, on one side, a function of effective stress through poroelasticity, i.e. increase in injection pressure while keeping the confining stress and backpressure constant. On the other side, coal swelling induced by CO_2 sorption also changes the fracture aperture and volume of the matrix blocks. The mechanisms of such behaviour will be discussed in detail in the following sections.

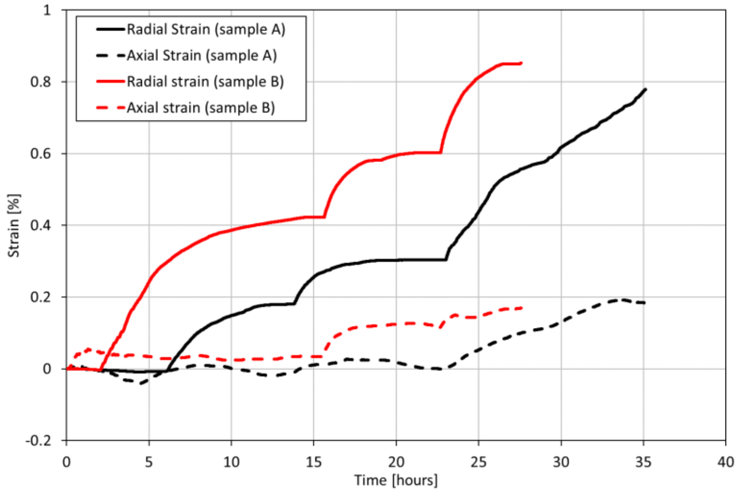

Fig. 8. Axial and radial strains determined during carbon dioxide injection on both samples.

3.2. Permeability to gases

In order to calculate the permeability to gases using Darcy's law (equation 1), a linear relationship between the pressure gradient and the volumetric flow rate needs to exist (Jasinge et al., 2011). Fig. 9 presents the correlation between the gas flow rates and injection pressures for samples A and B. The results show that for a non-sorbing He injection in both samples, the relationship is linear demonstrating that Darcy's law for the samples considered is valid. However, a deviation from the linear behaviour observed for CO_2 is due to the influence of changes induced by CO_2 sorption and swelling under the constant stress conditions as it affects the fracture aperture and the area available for flow.

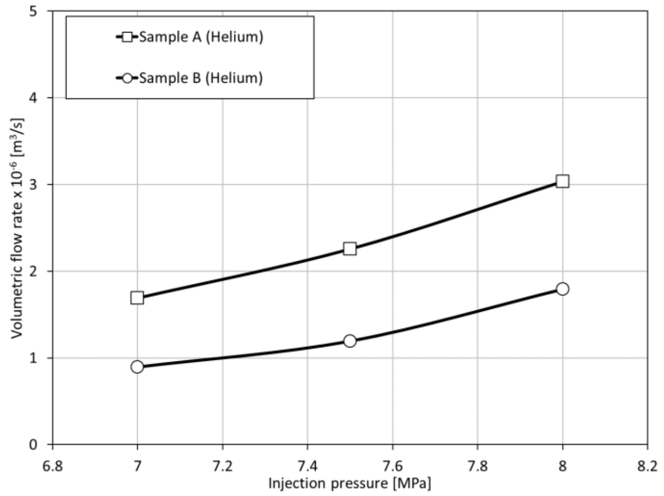

a)

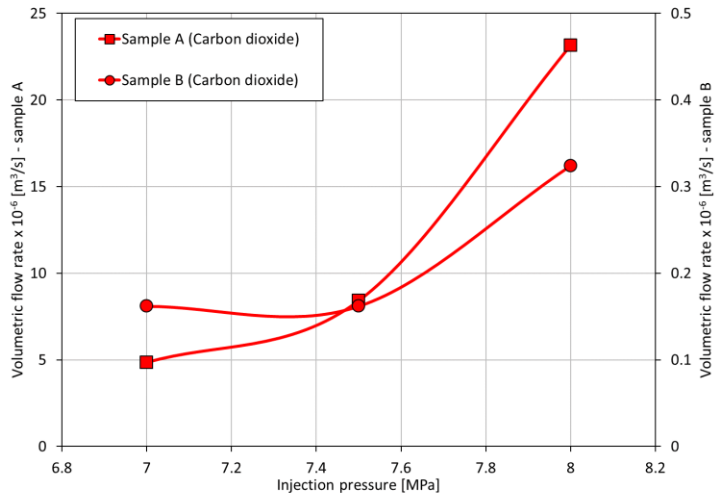

b)

Fig. 9. Gas flow rate versus injection pressure for samples A and B; a) during 1st He injection, b) during CO_2 injection.

It is commonly assumed that the same change of either confining pressure or pore gas pressure has the same impact on the effective stress change resulting in the effective stress coefficient being 1.0 (Seidle and Huitt, 1995). However, it has been shown that the effective stress coefficient is not constant and may be a function of pore pressure (Chen et al., 2011). As in this work, after the initial 4 hours of the experiment during which the pressures had been increased to the designed values, the injection pressure was the only variable, the permeability values of both samples to He and CO_2 plotted as a function of injection pressures are presented in Fig. 10. The permeability to He obtained on sample A varies between 1.53×10^{-16} m^2 to 1.15×10^{-16} m^2 and permeability to CO_2 from 3.87×10^{-17} m^2 to 1.07×10^{-17}, showing that CO_2 injection results in one order of magnitude lower permeability values than He injection. CO_2 permeability values up to two orders of magnitude lower than He permeability values were determined on sample B, i.e. the permeability to He is varying between 1.66×10^{-17} m^2 and 1.08×10^{-17} m^2 and the permeability to CO_2 is ranging from 4.03×10^{-19} to 2.58×10^{-19}. Such results imply that the permeability reduction due to CO_2 induced swelling was more pronounced in sample B than sample A.

An exponential functional form was used to estimate the variation permeability with injection gas pressure change under constant confining conditions, i.e. effective stress change (Pan et al., 2010; Chen et al., 2011; Meng et al., 2015). Based on the trendlines given in Fig. 10, permeabilities to He and CO_2 exhibit different behaviour. During He injection, the permeability follows an exponential law with the coefficients of determination being 0.99 and 0.97 for samples A and B, respectively. As mentioned earlier, the main cause of permeability change is the poroelastic response of the coal structure, which is supported by the volumetric strain change showing a strong linear dependency on injection pressure for both samples, with coefficients of determination being 0.98 for sample A and 0.99 for sample B. However, one can notice that the rates of change of both permeability and volumetric strain with an increase in gas pressure are higher in the case of sample B than sample A.

As discussed previously, CO_2 flow rates experienced only a partial recovery with an increase in injection pressure due to the coal swelling resulting in a non-linear dependency of permeability to CO_2 on injection pressure (Fig. 10b). Similarly, the volumetric strains follow an exponential relationship with the gas pressure, with coefficients of determination of 0.97 (sample A) and 0.99 (sample B) confirming that CO_2 sorption induces non-linear coal expansion. Permeability to CO_2 in sample B initially decreases by 12% (injection pressure 7.5 MPa) and then rebounds to a net increase of 56% (injection pressure 8.0 MPa) over the permeability of 2.58×10^{-19} measured at 7.0 MPa injection pressure. Although the CO_2 permeability evolution in sample A can be represented by an exponential law, one can observe that the permeability value obtained at 7.5 MPa injection pressure (1.61×10^{-17} m^2) is more than 10% lower than the expected permeability behaviour predicted by the trendline. Due to such behaviour, the coefficients of determination of 0.95 (sample A) and 0.56 (sample B) related to permeability evolution suggest that the exponential law might not realistically capture the CO_2 permeability behaviour under the constant stress conditions where permeability decreases at the beginning and then recovers to a level of permeability over the initial permeability. This is related to the fact that under the constant stress boundary condition, the initial permeability reduction is governed by the swelling of the coal matrix which narrows the fracture aperture

(Qu et al., 2014). This is then followed by a permeability rebound related to the swelling of the matrix reaching the external boundary after which the swelling area continues to increase in a local scale (Qu et al., 2014). Under such conditions, both matrix and fracture swell together making the fracture to reopen again and drive an increase in permeability (Qu et al., 2014).

However, opposite to the He injection case, the rates of change of both permeability and volumetric strain with an increase in injection pressure are now higher in the case of sample A than B. The underlaying reason for that could be related to the changes induced by CO_2 sorption, as sample A was exposed to higher flow and mean pressure of CO_2 than sample B, which will be further investigated and explained in the following sections.

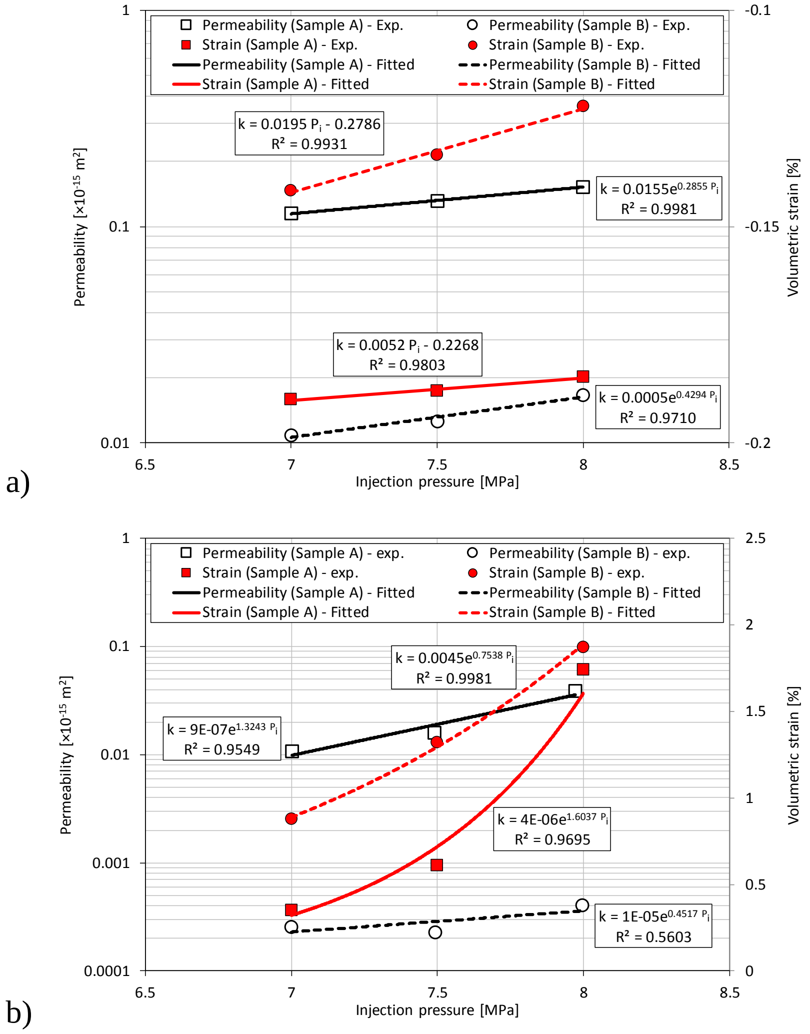

Fig. 10. Permeability and volumetric strains vs. injection pressure for samples A and B; a) during 1st He injection, b) during CO_2 injection.

3.3. Temperature changes

Fig. 11 presents the pressure difference between the inlet and outlet of the samples as well as the temperature recorded during the 1st He and CO_2 sequences. The results show that He flow experiments were performed under constant temperature conditions, i.e. 37±1°C. However, one can observe that the temperature measured on sample A showed a minor increase over the course of the experiment which can be associated with the Joule-Thomson effect as the He heats up by approximately 0.6 K/MPa upon expansion (Oldenburg, 2007; Linstrom and Mallard, 2016). Nevertheless, the measured change was within the experimental error margins of the measuring system.

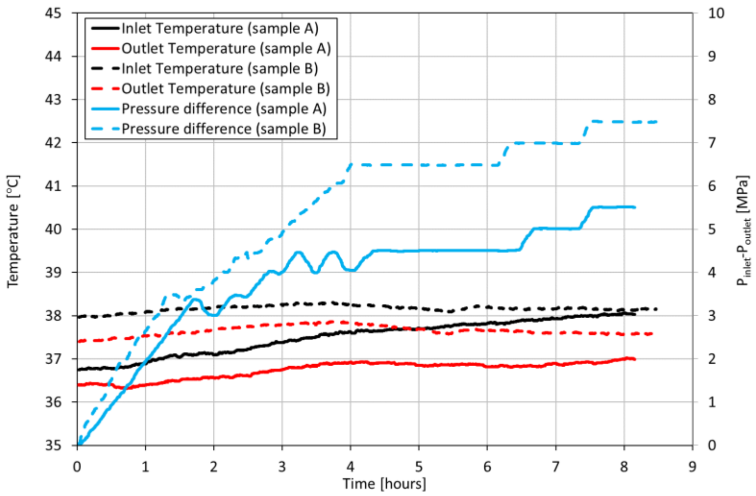

a)

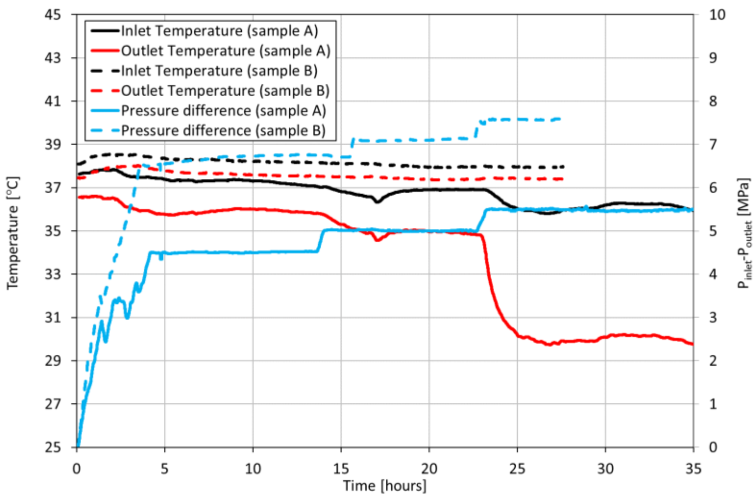

b)

Fig. 11. Experimental temperature and pressure difference between the inlet and outlet determined on both samples; a) during the 1st He injection, b) during CO_2 injection.

The results of temperature measurements during CO_2 injection show that the temperature measured on sample B was stable, staying in the region of 37±1°C. Opposite to that, temperature measured on sample A showed a continuous decrease over the course of the experiment with the most significant drop in temperature during the third injection stage (8.0 MPa injection pressure). In particular, when the supercritical CO_2 was injected into sample A, temperature reduced by 1.8°C and 6.8°C near the injection and production sides of the sample, respectively. Such behaviour is attributed to the cooling effect of CO_2 upon expansion, i.e. the Joule-Thomson effect (Oldenburg, 2007).

By analysing Fig. 11, it can be observed that the significant temperature changes recorded on sample A occurred at a pressure difference of 5.5 MPa. However, under a pressure difference of 7.6 MPa established within sample B at the end of the third injection step (8.0 MPa), no temperature reduction was recorded. The pressure gradient and amount of gas flowing across the samples are the main reasons for such difference in the behaviour. As shown earlier, up to 70 times lower flow rates were recorded in sample B than sample A (Fig. 7). This implies that the volume of pores conducting gas in sample B is smaller compared to sample A and hence, the heat provided by the confining oil and the heating elements can effectively diminish the cooling induced by gas expansion. On the contrary, flow rates above 100 g/h induced a measurable temperature change in sample A related to the cooling of the near-critical CO_2 which has been previously shown to be approximately 5-10 °C/MPa (Kazemifar and Kyritsis, 2014; Linstrom and Mallard, 2016). As the temperature data related to Joule-Thomson cooling effect reported in this work are lower than one would expect based on the literature data (e.g. Kazemifar and Kyritsis, 2014), the discrepancy in the results is related to the thermal properties of the materials, i.e. coal, PTFE tape and silicone sleeve used in this work. Therefore, as the temperature was measured by placing the thermocouple directly on the silicone sleeve, it can be inferred that the temperature drop within the coal sample would be higher. This is supported by the fact that the thermal conductivity of anthracite coal is low, i.e. 0.2-0.4 $W.m^{-1}.K^{-1}$ (e.g. Zhu et al., 2011; Liu et al., 2015).

Although this work did not include sorption capacity determination, it is known that gas adsorption is an exothermic process since energy is released during attractive interactions, with the heat of CO_2 adsorption being in the region of 25-28 kJ/mol and relatively independent of temperature and coal rank (Cao and Sircar, 2001; Ozdemir et al., 2004; White et al., 2005; Yue et al., 2015). Liu et al. (2015) demonstrated that CO_2 sorption on anthracite can induce changes up to 8.8 °C, and that such changes in temperature increase with an increase in injection pressure. In comparison, adsorption of CH_4 on anthracitic coal, which is evaluated to have the mean heat of adsorption of 23.3 kJ/mol (e.g. Tang et al., 2015), can induce a sudden increase in temperature of the coal sample up to 13.8 °C as shown by Yue et al. (2015). Hence, such temporary spike in temperature can partially offset the Joule-Thomson effect and the combination of these two phenomena on the thermal state of the system needs to be considered.

It has been previously demonstrated that sorption capacity to CO_2 and the resulting swelling of high rank coals are inversely proportional to temperature (e.g. Krooss et al., 2002; Sakurovs et al., 2008; Battistutta et al., 2010; Baran et al., 2015). Furthermore, the reduction in temperature shrinks the coal matrix (Liu et al., 2015). Therefore, such temperature related changes within the coal structure during CO_2 injection could affect the deformation and transport properties of coal. While thermal contraction of the coal matrix would enhance the flow of CO_2 by widening the flow paths, increase in the amount of CO_2 adsorbed during the temperature drop period would increase the coal swelling and restrict the gas flow by reducing the aperture of the fractures. The decrease in temperature could also be responsible for the fact that sample A did not achieve complete steady state in the given experimental time, as shown in Fig. 7 and Fig. 8., as the decrease in temperature causes an increase in equilibrium time related to the decrease in diffusion rates (e.g. Charrière et al., 2010).

Moreover, coals and in particular of high-rank exhibit reduction of elastic modulus and uniaxial compressive strength up to 80% through inducement of new fractures and enhancement of the existing ones as a result of subcritical and supercritical CO_2 injection (Vishal et al., 2015; Zagorščak and Thomas, 2018). Hence, such reductions in deformation and strength properties of coals could be even more pronounced when the temperature of the system drops as the sorption and swelling increase. Furthermore, creation of new fractures and flow paths could be initiated by thermal stresses as a result of rapid cooling and induced coal swelling caused by an increase in CO_2 adsorption due to sudden reduction in temperature. The results observed on sample A, which experienced sudden increase in flow rates and expansion in the third injection step and not reaching the steady-state in the experimental time given, can be then explained by such complex coupled processes.

3.4. Relationship between the flow of CO_2 and the sorption induced volumetric swelling

The normalised values of flow rates and volumetric strains over time duration of the experiments on both samples are shown in Fig. 12 to analyse how the coal volumetric swelling affects the gas transport. During the first 18% and 8% of experimental time, samples A and B showed minor volumetric response, respectively. In particular, sample A experiences minor compression, up to the 3% of the maximum volumetric strain while sample B expands by 2% of the maximum volumetric strain observed. However, after 8% (sample A) and 4% (sample B) of experimental time, the flow rates have already started to drop.

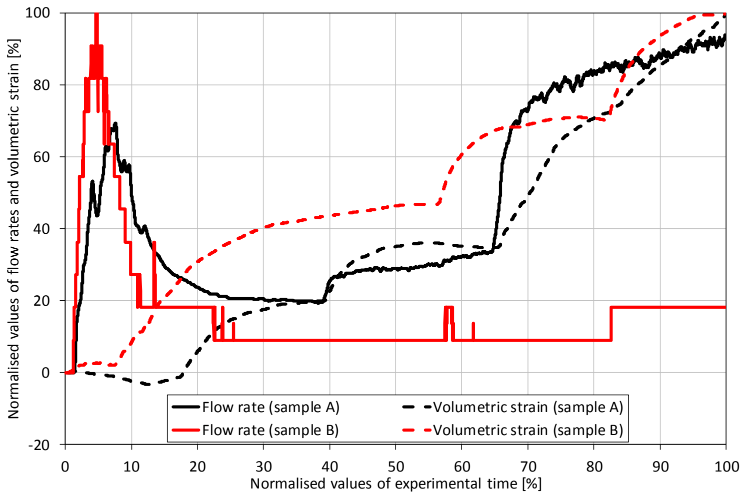

Fig. 12. Flow rate and volumetric strain time series for CO_2 injection in both samples.

The mechanisms for such behaviour can be explained through the concept where the matrix swelling first occurs locally, reducing the aperture of the fractures and then it transits into global swelling controlled by the external boundary, as suggested previously in the literature (Liu et al., 2011; Chen et al., 2013; Qu et al., 2012; 2014). During the initial injection of CO_2, i.e. up to first 8% (sample A) and 4% (sample B) of experimental time, only fractures are occupied by the gas which increases the gas pressure in the fractures resulting in a sudden increase in flow rates. As the CO_2 injection continues, CO_2 diffuses into the matrix increasing the gas pressure within it. Consequently, the matrix area in close vicinity to the fracture starts to swell reducing the fracture aperture and the area available for gas flow. Hence, this reduction negatively impacts the fracture permeability, as demonstrated for sample A and B which experience a rapid reduction in flow rates within 8-18% and 4-8% of experimental time, respectively. Although the flow rates observed are a net result of the permeability increase due to the increase in gas pressure and the reduction of fracture aperture due to swelling, the latter one has a higher impact than the former one. During this time, the swelling predominantly occurs locally, and the external boundary stays unmoved which is similar to the constant volume boundary case.

After that, as CO_2 diffuses further into the matrix and the swelling front moves away from the fracture, the impact of sorption induced swelling on the fracture aperture decreases. By increasing the matrix swelling area, the swelling pressure exceeds the value of the limiting pressure and the external boundary starts to move outwards. This is visible in 18-40% of experimental time for sample A and 8-55% of experimental for sample B where a sudden increase in volumetric strains with further injection of CO_2 is observed, but at the same time, the reduction in flow rates becomes more gradual reaching a steady-state at the end.

Increasing the injection pressure and decreasing the effective stress in turn, to initiate higher flow rates, after 40% (sample A) and 55% (sample) of experimental time until the end of the experiments proved to have less effect in sample B than sample A. As the coal matrix is not completely separated by the fractures, but some matrix blocks are mutually connected by the coal bridges (e.g. Liu et al., 2011), one can infer that the interconnectivity of these blocks and matrix properties govern the coal response. Qu et al. (2014) have suggested that both the coal matrix and bridges swell. Where the matrix blocks are completely separated by a fracture, sorption induced swelling of the blocks narrows the gap between matrix-faces and reduces permeability. If the blocks are connected via the bridges, swelling of those bridges enlarges the fracture aperture and increases permeability (Qu et al., 2014). Hence, as sample A has a visible well-developed fracture network (Fig. 2), it can be inferred that there are more coal blocks and bridges than in sample B that can be directly exposed to CO_2. Combined with the multiple processes induced by changes in thermal state of the system, as discussed in the earlier section, flow rates in sample A rebound earlier and at a higher rate than in sample B with poor fracture network and no visible changes in thermal state of the system. These findings support the work of Qu et al. (2014) who have numerically demonstrated that low temperature CO_2 injection results in earlier permeability rebound than high temperature CO_2 injection as the coal matrix shrinks due to thermal contraction as well as more gas adsorbs on the coal surface increasing the pressure in the coal matrix faster.

3.5. Reversibility of the CO_2 sorption induced changes

The results presented in Fig. 13 show that He flow rates recorded at the end of the second He injection sequence are 17 g/h and 2 g/h in samples A and B, respectively. Compared to the results obtained at the end of the first He injection sequence, 60-66% lower flow rates were observed. However, the volumetric response of both samples showed similar behaviour as the difference in the volumetric strain experienced during each sequence was negligible. In particular, sample A compressed by 0.19% and 0.20% during the first four hours of the first and second He injection sequences, respectively. After that, a minor expansion of 0.005% occurred in both injection sequences resulting from the injection pressure increase from 7.0 MPa to 8.0 MPa.

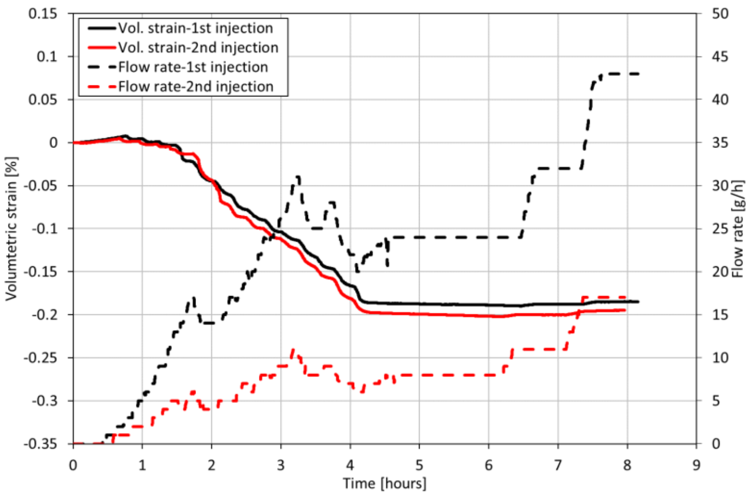

a)

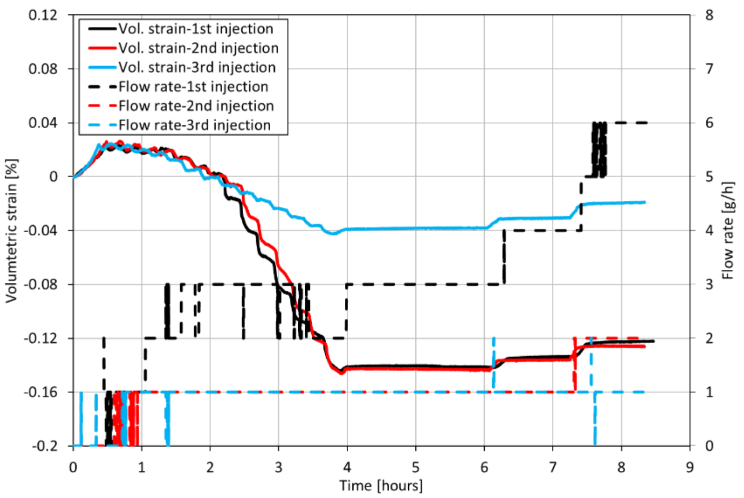

b)

Fig. 13. Volumetric strains and flow rates measured during different helium injection sequences; a) before and after CO_2 injection in sample A, b) before and after CO_2 injection, and after N_2 injection in sample B.

Following the saturation of sample B with N_2 for 48 hours and then degassing it, He flow rates during the 3rd He injection show a very similar trend to the flow rates obtained during the 2nd He injection after the sample has been treated with CO_2, demonstrating that there is no recovery in permeability as a result of N_2 sorption. Regarding the volumetric compression during the initial increase in pressures to reach the designed values, sample B experienced compression of 0.039% compared to the first two He injection sequences where the compression was 0.14%. Upon reaching the designed pressure conditions after 4 hours, qualitative and quantitative behaviour of the third He injection sequence was then the same as in the first two, i.e. sample expanded by 0.02% when the injection pressure increased by 1 MPa. Hence, it appears that such initial volumetric compression of the sample in the third He injection sequence, which could be associated with the creep of the coal during long-term loading, did not affect the flow behaviour.

Such observations for high rank coal are contrary to the studies performed by other researchers (e.g. Fujioka et al., 2010; Perera et al., 2011; Ranathunga et al., 2017) who have reported that N_2 injection in low rank coals can partially reverse the CO_2 sorption induced swelling and enhance permeability. A potential explanation could be related to the coal structure of high-rank coals and the difference in diameters of the N_2 and CO_2 molecules. In particular, high rank coals contain predominantly micropores making it more difficult for N_2, with relatively larger kinetic diameter than CO_2, to diffuse and adsorb into meso- and micropores easily accessible to CO_2 (Cui et al., 2004; White et al., 2005; Moore, 2012).

4. Conclusions

This paper presented the experimental results obtained from continuous and simultaneous measurements of flow rates, gas and confining pressures, temperature, radial and axial strains obtained during high-pressure injection of CO_2, He and N_2 in two high rank coal samples under constant confining stress conditions. Based on the experimental results obtained, the following conclusions were drawn:

- He injection resulted in continuous increase in flow rates and sample expansion with steady-state being achieved in less than half an hour after each injection step. As He is a non-sorbing gas, changes in effective stress, grain compressibility and the consequent increase in fracture aperture were the main mechanisms responsible for such behaviour.

- During CO_2 injection, several stages were identified. Initial CO_2 injection induced rapid increase in flow rates associated with a quick gas pressure build-up in the fractures, followed by a gradual decline in flow rates. This period of reduction in flow rates coincided with the period where negligible volumetric deformation of samples could be recorded. This demonstrated that the closure of fractures and the resulting decrease in permeability are primarily related to the internal (local) swelling of the coal structure. As the injection pressure was increased further, the samples experienced measurable global swelling resulting in the recovery of flow rates, which was particularly visible in sample A with well-developed fracture network.

- Temperature measurements on sample A showed a temperature drop during high flow of CO_2 associated with the Joule-Thomson effect. As sample A experienced higher increase in flow rates and expansion during this temperature reduction period compared to sample B, it was concluded that such abrupt change in the thermal state of system could have induced physical and chemical changes. In particular, a combination of different mechanisms such as increase in coal swelling and reduction of mechanical properties associated with an increase in sorption capacity with a decrease in temperature, thermally induced cracking as well as thermal contraction were named to be responsible for such behaviour.

- Coal expansion was more dominant in case of CO_2 injection than in case of He injection, i.e. differences of more than one order of magnitude were recorded. The permeability to CO_2 (3.9×10^{-17} m^2 to 2.6×10^{-19} m^2) was one to two orders of magnitude lower than permeability to He (1.5×10^{-16} m^2 to 1×10^{-17} m^2) as a result of the CO_2 sorption induced changes.

- The changes induced by CO_2 sorption were detrimental on coal permeability to non-sorptive gas, reducing it by 60-66%. Furthermore, N_2 sorption could not reverse those changes, contrary to some previous findings in the literature on the effectiveness of N_2 on the permeability enhancement.

This work demonstrated that high-rank coal seams with pre-existing highly developed fracture network are suitable for CO_2 injection, and although can experience an initial decline in flow rates, the recovery could be expected over time with further increase in injection pressure as a result of complex interactions occurring during the CO_2 injection process. On the contrary, high-rank coals with poorly developed fracture network are strongly affected by the CO_2 sorption induced swelling and do pose a challenge in storing CO_2. Hence, the existing cleats should be enhanced, and new ones created through forms of stimulation prior to or during the injection of CO_2 as the N_2 injection proves to be inefficient in reversing the changes induced by CO_2 sorption in high-rank coals. However, in both cases, the impact of complex mechanisms induced by potential temperature variations of the system, especially near the injection point, that can induce changes in the sorptive potential of coals to CO_2 and related impacts on the coal deformation and strength properties should be evaluated when assessing the storage potential of the target coal seams. Moreover, considering temperature related changes in the stress state and potential freezing of the residual water or creation of CO_2 and CH_4 hydrates is important while analysing the injectivity and stability of the storage system.

Overall, the experimental findings presented in this work support the theoretical framework previously suggested in the literature (e.g. Qu et al., 2014) and offer a great prospect to be further exploited for validation of developed numerical models which provide reliable platforms for predicting the behaviour of gas-storage system.

5. Acknowledgements

This work was carried out as a part of SEREN and FLEXIS Projects. Both projects have been part-funded by the European Regional Development Fund through the Welsh Government. The financial support, for the first author, is gratefully acknowledged. The authors wish to express their appreciation to Celtic Energy Ltd for providing coal blocks to conduct this research.

6. References

1. Alexis, D.A., Karpyn, Z.T., Ertekin, T. and Crandall, D. 2015. Fracture permeability and relative permeability of coal and their dependence on stress conditions. *Journal of Unconventional Oil and Gas Resources*, 10, pp. 1-10.

2. Anggara, F., Sasaki, K. and Sugai, Y. 2016. The correlation between coal swelling and permeability during CO_2 sequestration: A case study using Kushiro low rank coals. *International Journal of Coal Geology*, 166, pp. 62-70.

3. ASTM Standards, 2015. *ASTM D3302/D3302M. Standard Test Method for Total Moisture in Coal. Vol. 05.06.* West Conshohocken, PA: ASTM International.

4. ASTM Standards, 2015. *ASTM D388. Standard Classification of Coals by Rank. Vol. 05.06.* West Conshohocken, PA: ASTM International.

5. Baran, P., Zarębska, K. and Bukowska, M. 2015. Expansion of Hard Coal Accompanying the Sorption of Methane and Carbon Dioxide in Isothermal and Non-isothermal Processes. *Energy & Fuels*, 29(3), pp. 1899-1904.

6. Battistutta, E., van Hemert, P., Lutynski, M., Bruining, H. and Wolf, K.H. 2010. Swelling and sorption experiments on methane, nitrogen and carbon dioxide on dry Selar Cornish coal. *International Journal of Coal Geology*, 84(1), pp. 39-48.

7. Biot, M.A. 1941. General theory of three-dimensional consolidation. *Journal of Applied Physics*, 12 (2), pp. 155-164.

8. Cai, Y., Liu, D., Pan, Z., Yao, Y., Li, J. and Qiu, Y. 2013. Pore structure and its impact on CH_4 adsorption capacity and flow capability of bituminous and subbituminous coals from Northeast China. *Fuel*, 103, pp. 258-268.

9. Cao, D.V. and Sircar, S. 2001. Temperature dependence of the isosteric heat of adsorption. *Adsorption Science & Technology*, 19(10), pp. 887-894.

10. Charrière, D., Pokryszka, Z. and Behra, P. 2010. Effect of pressure and temperature on diffusion of CO_2 and CH_4 into coal from the Lorraine basin (France). *International Journal of Coal Geology*, 81, pp. 373-380.

11. Chen, Z., Pan, Z., Liu, J., Connell, L.D. and Elsworth, D. 2011. Effect of the effective stress coefficient and sorption-induced strain on the evolution of coal permeability: Experimental observations. *International Journal of Greenhouse Gas Control*, 5(5), pp. 1284-1293.

12. Chen, Z., Liu, J., Elsworth, D., Pan, Z. and Wang, S. 2013. Roles of coal heterogeneity on evolution of coal permeability under unconstrained boundary conditions. *Journal of Natural Gas Science and Engineering*, 15, pp. 38-52.

13. Cui, X., Bustin, R.M. and Dipple, G. 2004. Selective transport of CO_2, CH_4 and N_2 in coals: insights from modeling of experimental gas adsorption data. *Fuel*, 83(3), pp. 293-303.

14. Day, S., Fry, R. and Sakurovs, R., 2008. Swelling of Australian coals in supercritical CO_2. *International Journal of Coal Geology*, 74(1), pp. 41-52.

15. Day, S., Fry, R., Sakurovs, R. and Weir, S. 2010. Swelling of Coals by Supercritical Gases and Its Relationship to Sorption. *Energy & Fuels*, 24, pp. 2777-2783.

16. Durucan, S. and Edwards, J.S. 1986. The effects of stress and fracturing on permeability of coal. *Mining Science and Technology*, 3, pp. 205-216.

17. Fujioka, M., Yamaguchi, S. and Nako, M. 2010. CO_2-ECBM field tests in the Ishikari Coal Basin of Japan. *International Journal of Coal Geology*, 82(3-4), pp. 287-298.

18. Gathitu, B.B., Chen, W.Y. and McClure, M. 2009. Effects of Coal Interaction with Supercritical CO_2: Physical Structure. *Industrial & Engineering Chemistry Research*, 48(10), pp. 5024-5034.

19. He, J., Shi, Y., Ahn, S., Kang, J.W. and Lee, C. 2010. Adsorption and desorption of CO_2 on Korean coal under subcritical to supercritical conditions. *The Journal of Physical Chemistry*, 114(14), pp. 4854-4861.

20. Hol, S., Peach, C.J. and Spiers, C.J. 2011. Applied stress reduces the CO_2 sorption capacity of coal. *International Journal of Coal Geology*, 85, pp. 128-142.

21. Hol, S. and Spiers, C.J. 2012. Competition between adsorption-induced swelling and elastic compression of coal at CO_2 pressures up to 100 MPa. *Journal of the Mechanics and Physics of Solids*, 60, pp. 1862-1882.

22. Hol, S., Spiers, C.J. and Peach, C.J. 2012a. Microfracturing of coal due to interaction with CO_2 under unconfined conditions. *Fuel*, 97, pp. 569-584.

23. Hol, S., Peach, C.J. and Spiers, C.J. 2012b. Effect of 3-D stress state on adsorption of CO_2 by coal. *International Journal of Coal Geology*, 93, pp. 1-15.

24. Hol, S., Gensterblum, Y. and Massarotto, P. 2014. Sorption and changes in bulk modulus of coal – experimental evidence and governing mechanisms for CBM and ECBM applications. *International Journal of Coal Geology*, 128-129, pp. 119-133.

25. IEA, 2016. *20 Years of Carbon Capture and Storage. Accelerating Future Deployment.* International Energy Agency, Paris, France.

26. IPCC, 2014. *Climate Change 2014: Synthesis Report*. Intergovernmental Panel on Climate Change.

27. IPCC, 2018. *Global warming of 1.5°C. An IPCC Special Report on the impacts of global warming of 1.5°C above pre-industrial levels and related global greenhouse gas emission pathways, in the context of strengthening the global response to the threat of climate change, sustainable development, and efforts to eradicate poverty.* Intergovernmental Panel on Climate Change.

28. Jasinge, D., Ranjith, P.G. and Choi, S.K. 2011. Effects of effective stress changes on permeability of latrobe valley brown coal. *Fuel*, 90, pp. 1292-1300.

29. Kazemifar, F. and Kyritsis, D. 2014. Experimental investigation of near-critical CO_2 tube-flow and Joule-Thomson throttling for carbon capture and sequestration. *Experimental Thermal and Fluid Science*,53, pp. 161-170.

30. Krooss, B.M., van Bergen, F., Gensterblum, Y., Siemons, N., Pagnier, H.J.M. and David, P. 2002. High-pressure methane and carbon dioxide adsorption on dry and moisture-equilibrated Pennsylvanian coals. *International Journal of Coal Geology*, 51 (2), pp. 69-92.

31. Levine, J.R. 1996. Model study of the influence of matrix shrinkage on absolute permeability of coal bed reservoirs. *Geological Society, London, Special Publications*, 109, pp. 197-212.

32. Li, D., Liu, Q., Weniger, P., Gensterblum, Y., Busch, A. and Krooss, B.M. 2010. High-pressure sorption isotherms and sorption kinetics of CH_4 and CO_2 on coals. *Fuel*, 89, pp. 569-580.

33. Li, J., Liu, D., Yao, Y., Cai, Y. and Chen, Y. 2013. Evaluation and modeling of gas permeability changes in anthracite coals. *Fuel*, 111, pp. 606-612.

34. Linstrom, P.J. and Mallard, W.G., Eds. NIST Chemistry WebBook, NIST Standard Reference Database Number 69, National Institute of Standards and Technology, Gaithersburg MD, 20899, http://webbook.nist.gov, (retrieved October 20, 2016).

35. Liu, J., Wang, J., Chen, Z., Wang, S., Elsworth, D. and Jiang, Y. 2011. Impact of transition from local swelling to macro swelling on the evolution of coal permeability. *International Journal of Coal Geology,* 88(1), pp. 31-40.

36. Liu, Z., Feng, Z., Zhang, Q., Zhao, D. and Guo, H. 2015. Heat and deformation effects on coal during adsorption and desorption of carbon dioxide. *Journal of Natural Gas Science and Engineering*, 25, pp. 242-252.

37. Liu, Q., Cheng, Y., Ren, T., Jing, H., Tu, Q. and Dong, J. 2016. Experimental observations of matrix swelling area propagation on permeability evolution using natural and reconstituted samples. *Journal of Natural Gas Science and Engineering*, 34, pp. 680-688.

38. Majewska, Z., Ceglarska-Stefańska, G., Majewski, S. and Ziętek, J., 2009. Binary gas sorption/desorption experiments on a bituminous coal: Simultaneous measurements on sorption kinetics, volumetric strain and acoustic emission. *International Journal of Coal Geology*, 77(1), pp. 90-102.

39. Mazumder, S. and Wolf, K.H. 2008. Differential swelling and permeability change of coal in response to CO_2 injection for ECBM. *International Journal of Coal Geology*, 74, pp. 123-128.

40. Meng, Y., Li, Y. and Lai, F. 2015. Experimental study on porosity and permeability of anthracite coal under different stresses. *Journal of Petroleum Science and Engineering*, 133, pp. 810-817.

41. Mohammad, S., Fitzgerald, J., Robinson Jr., R.L. and Gasem, K.A.M. 2009. Experimental Uncertainties in Volumetric Methods for Measuring Equilibrium Adsorption. *Energy & Fuels*, 23, pp. 2810-2820.

42. Moore, T.A. 2012. Coalbed methane: A review. *International Journal of Coal Geology*, 101, pp. 36-81.

43. Oldenburg, C.M. 2007. Joule-Thomson cooling due to CO_2 injection into natural gas reservoirs. *Energy Conversion and Management*, 48(6), pp. 1808-1815.

44. Ozdemir, E., Morsi, B.I. and Schroeder, K. 2004. CO_2 adsorption capacity of argonne premium coals. *Fuel*, 83, pp. 1085-1094.

45. Pan, Z., Connell, L.D. and Camilleri, M. 2010. Laboratory characteristics of coal reservoir permeability for primary and enhanced coalbed methane recovery. *International Journal of Coal Geology*, 82(3), pp. 252-261.

46. Pan, Z. and Connell, L.D. 2011. Modelling of anisotropic coal swelling and its impact on permeability behaviour for primary and enhanced coalbed methane recovery. *International Journal of Coal Geology*, 85, 257-267.

47. Perera, M.S.A., Ranjith, P.G., Airey, D.W. and Choi, S.K. 2011. Sub- and super-critical carbon dioxide flow behavior in naturally fractured black coal: An experimental study. *Fuel*, 90, pp. 3390-3397.

48. Prinz, D. and Littke, R. 2005. Development of the micro- and ultramicroporous structure of coals with rank as deduced from the accessibility to water. *Fuel*, 84, pp. 1645-1652.

49. Qu, H., Liu, J., Chen, Z., Wang, J., Pan, Z., Connell, L. and Elsworth, D. 2012. Complex evolution of coal permeability during CO_2 injection under variable temperatures. *International Journal of Greenhouse Gas Control*, 9, pp. 281-293.

50. Qu, H., Liu, J., Pan, Z. and Connell, L. 2014. Impact of matrix swelling area propagation on the evolution of coal permeability under coupled multiple processes. *Journal of Natural Gas Science and Engineering*, 18, pp. 451-466.

51. Ranathunga, A.S., Perera, M.S.A., Ranjith, P.G., Zhang, X.G. and Wu, B. 2017. Super-critical carbon dioxide flow behaviour in low rank coal: A meso-scale experimental study. *Journal of CO_2 Utilization*, 20, pp. 1-13.

52. Sakurovs, R., Day, S., Weir, S. and Duffy, G. 2008. Temperature dependence of sorption of gases by coals and charcoals. *International Journal of Coal Geology*, 73, pp. 250-258.

53. Sakurovs, R., Day, S. and Weir, S. 2009. Causes and consequences of errors in determining sorption capacity of coals for carbon dioxide at high pressure. *International Journal of Coal Geology*, 77, pp. 16-22.

54. Seidle, J.R. and Huitt, L.G. 1995. Experimental measurement of coal matrix shrinkage due to gas desorption and implications for cleat permeability increases. *International Meeting on Petroleum Engineering.* Society of Petroleum Engineers.

55. Tang, X., Wang, Z., Ripepi, N., Kang, B. and Yue, G. 2015. Adsorption affinity of different types of coal: Mean Isosteric Heat of Adsorption. *Energy & Fuels*, 29, pp. 3609-3615.

56. The Royal Society and Royal Academy of Engineering. 2018. *Greenhouse Gas removal*. Report.

57. Van Bergen, F., Krzystolik, P., van Wageningen, N., Pagnier, H., Jura, B., Skiba, J., Winthaegen, P. and Kobiela, Z. 2009. Production of gas from coal seams in the Upper Silesian Coal Basin in Poland in the post-injection period of an ECBM pilot site. *International Journal of Coal Geology*, 77(1-2), pp. 175-187.

58. Vishal, V. 2017. In-situ disposal of CO_2: Liquid and supercritical CO_2 permeability in coal at multiple down-hole stress conditions. *Journal of CO_2 Utilization*, 17, pp. 235-242.

59. Vishal, V., Ranjith, P.G. and Singh, T.N. 2015. An experimental investigation on behaviour of coal under fluid saturation, using acoustic emission. *Journal of Natural Gas Science and Engineering*, 22, pp. 428-436.

60. Wang, G.X., Wei, X.R., Wang, K., Massarotto, P. and Rudolph, V. 2010. Sorption-induced swelling/shrinkage and permeability of coal under stressed adsorption/desorption conditions. *International Journal of Coal Geology*, 83, pp. 46-54.

61. Wang, J.G., Liu, J. and Kabir, A. 2013. Combined effects of directional compaction, non-Darcy flow and anisotropic swelling on coal seam gas extraction. *International Journal of Coal Geology*, 109-110, pp. 1-14.

62. Wang, L., Wang, Z., Li, K. and Chen, H. 2015. Comparison of enhanced coalbed methane recovery by pure N_2 and CO_2 injection: Experimental observations and numerical simulation. *Journal of Natural Gas Science and Engineering*, 23, pp. 363-372.

63. White, C.M., Smith, D.H., Jones, K.L., Goodman, A.L., Jikich, S.A., Lacount, R.B., Dubose, S.B., Ozdemir, E., Morsi, B., Schroeder, K.T. 2005. Sequestration of Carbon Dioxide in Coal with Enhanced Coalbed Methane Recovery – A Review. *Energy&Fuels*, 19 (3), 659-724.

64. Wong, S., Law, D., Deng, X., Robinson, J., Kadatz, B., Gunter, W.D., Jianping, Y., Sanli, F. and Zhiqiang, F. 2007. Enhanced coalbed methane and CO_2 storage in anhracitic coals – Micro-pilot test at Sout Qinshui, Shanxi, China. *International Journal of Greenhouse Gas Control*, 1, pp. 215-222.

65. Yue, G., Wang, Z., Tang, X., Li, H. and Xie, C. 2015. Physical Simulation of Temperature Influence on Methane Sorption and Kinetics in Coal (II): Temperature Evolvement during Methane Adsorption in Coal Measurement and Modeling. *Energy & Fuels*, 29, pp. 6355-6362.

66. Zagorščak, R. and Thomas, H.R. 2016. Experimental study of the Klinkenberg Effect on the Gas Permeability of Coal. *Diffusion Foundations*, 10, pp. 83-92.

67. Zagorščak, R. 2017. *An Investigation of Coupled Processes in Coal in Response to High Pressure Gas Injection.* Ph.D. Thesis, Cardiff University, Wales, UK.

68. Zagorščak, R. and Thomas, H.R. 2018. Effects of subcritical and supercritical CO_2 sorption on deformation and failure of high-rank coals. *International Journal of Coal Geology*, 199, pp. 113-123.

69. Zagorščak, R. and Thomas, H.R. 2019. High-pressure CO_2 Excess Sorption Measurements on Powdered and Core Samples of High-Rank Coals from Different Depths and Locations of the South Wales Coalfield. *Energy & Fuels*, 33(7), pp. 6515-6526.

70. Zhou, F., Hussain, F. and Cinar, Y. 2013. Injecting pure N_2 and CO_2 to coal for enhanced coalbed methane: Experimental observations and numerical simulation. *International Journal of Coal Geology*, 116-117, pp. 53-62.

71. Zhu, W.C., Wei, C.H, Liu, J., Qu, H.Y. and Elsworth, D. 2011. A model of coal-gas interaction under variable temperatures. *International Journal of Coal Geology*, 86(2-3), pp. 213-221.